

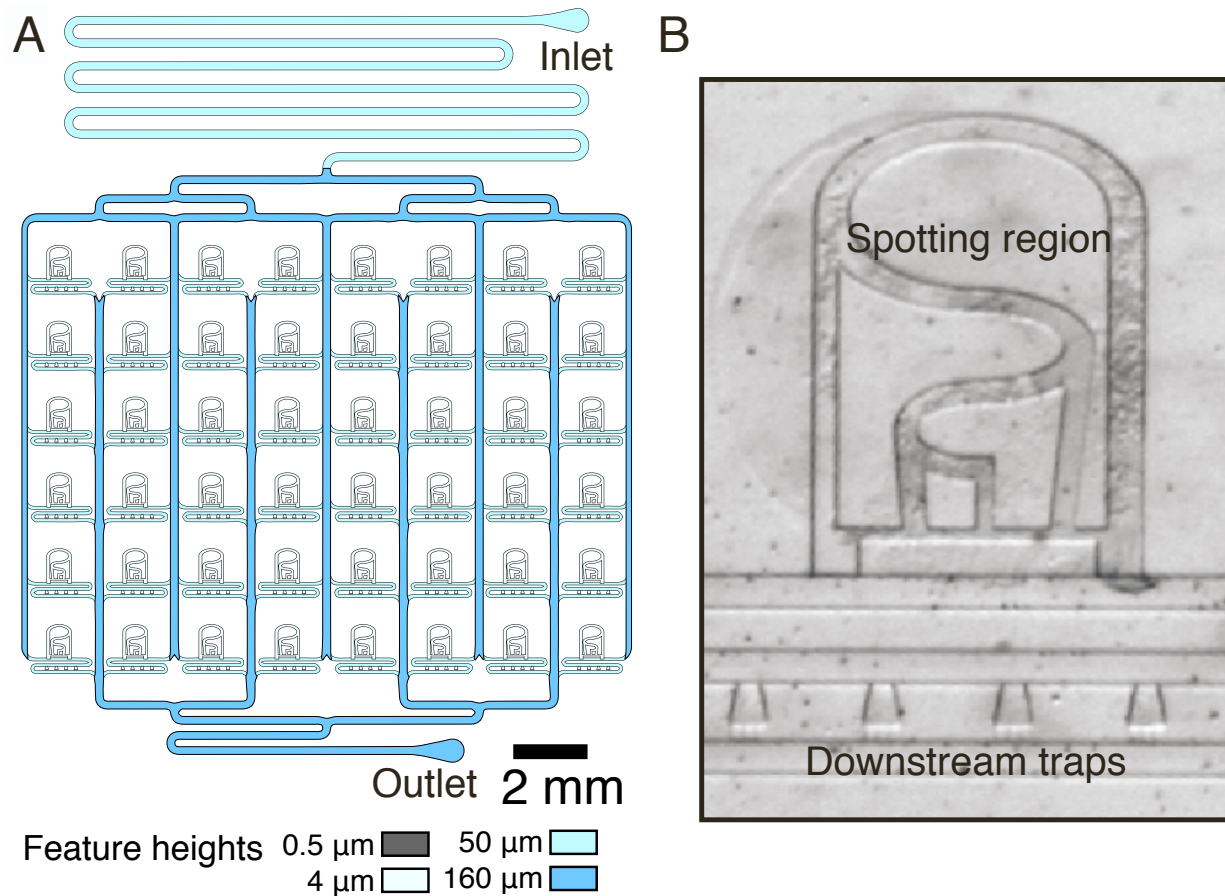
Cell Systems, Volume 13

Supplemental information

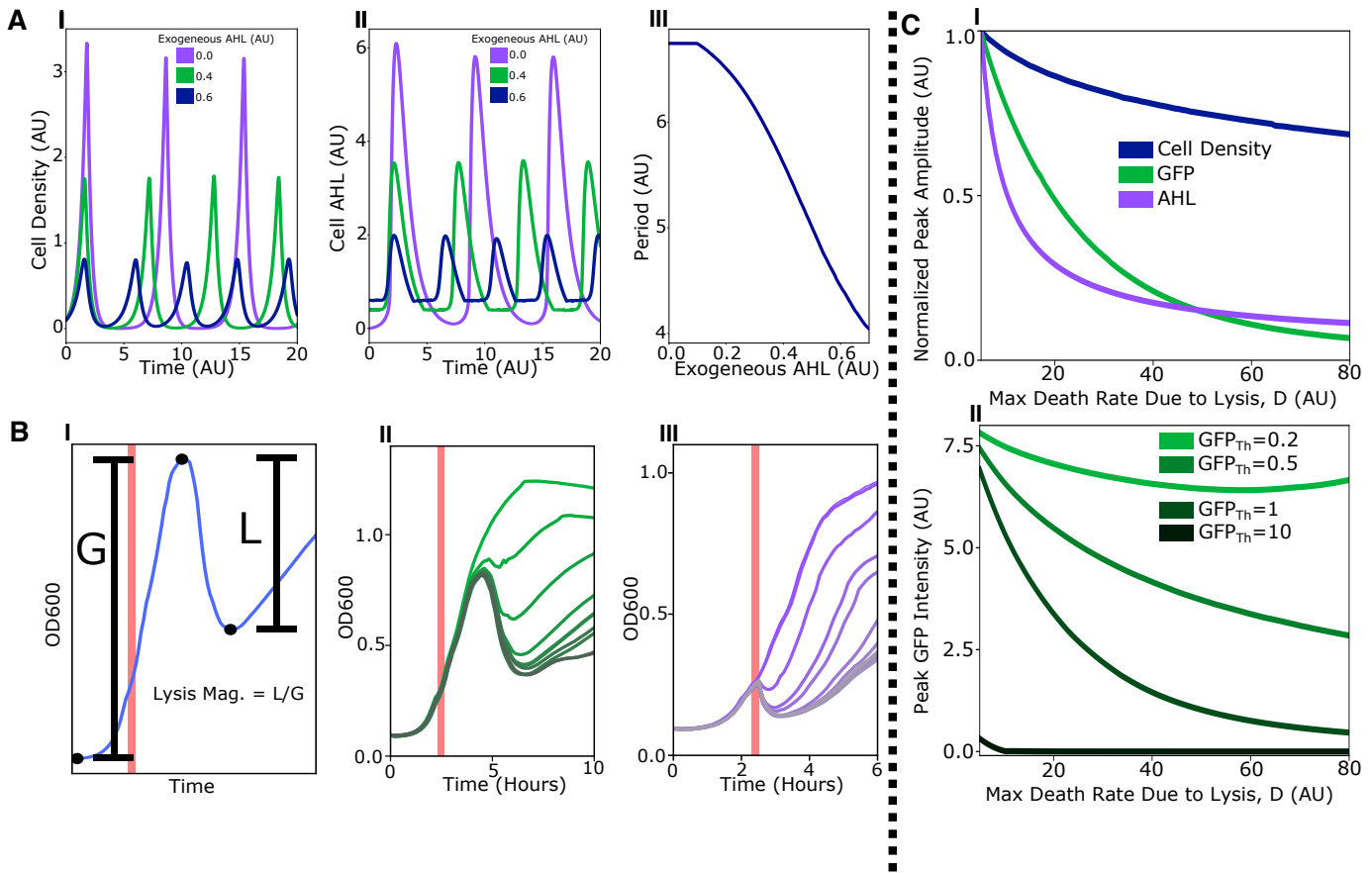
**Design, mutate, screen: Multiplexed
creation and arrayed screening
of synchronized genetic clocks**

Andrew Lezia, Nicholas Csicsery, and Jeff Hasty

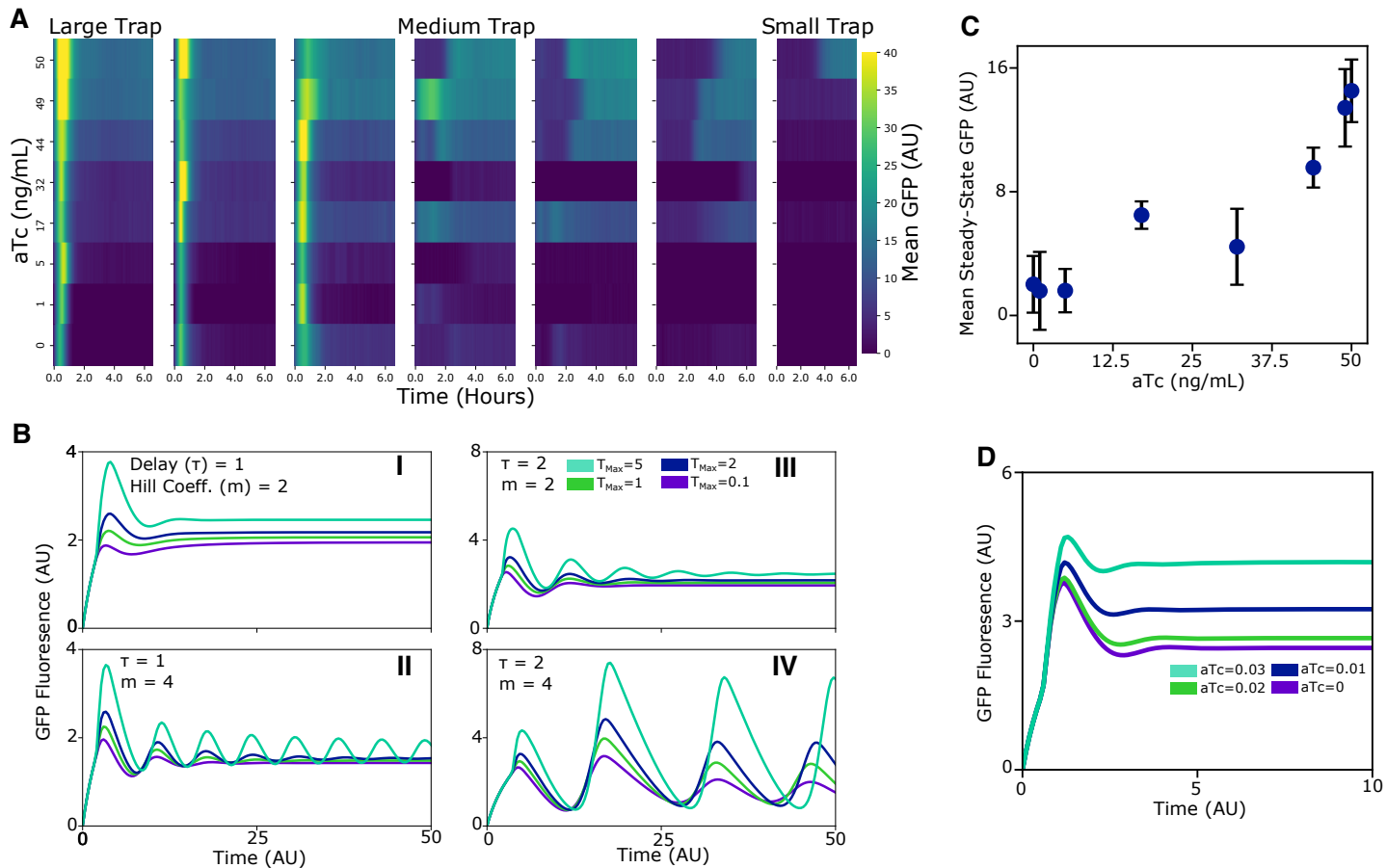
SI Figures



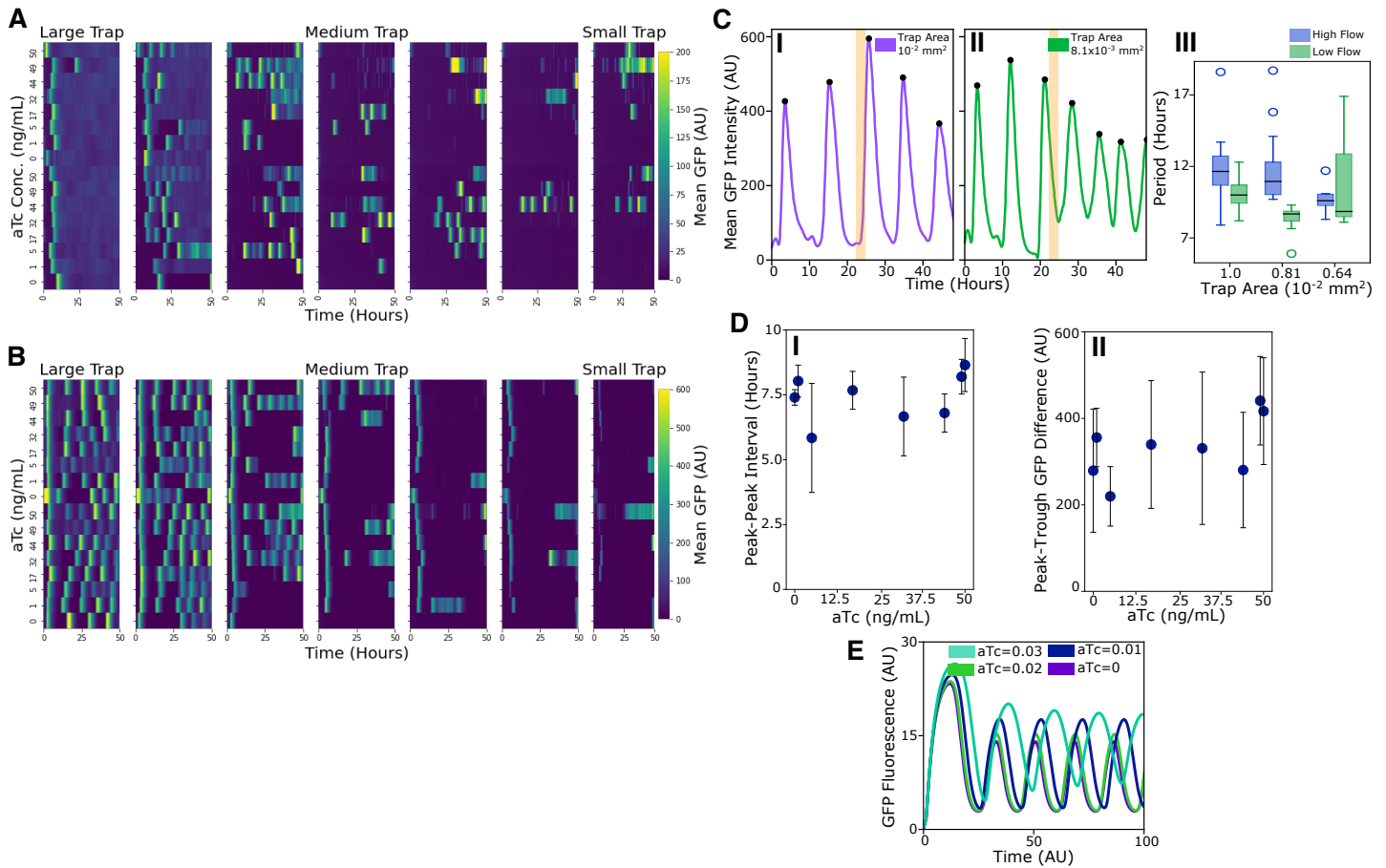
SI Figure 1: A 48-position microfluidic device (Supplementary data related to Figure 1 and STAR Methods Section) (A) The multiplexed chip used in this paper consists of 48 individually loadable cell trapping regions (4 μm). PDMS devices are exposed to oxygen plasma, loaded with cells, and then bonded to a glass slide. Cells were deposited onto the microfluidic chip from liquid cultures by acoustic droplet ejection with a Labcyte Echo 550. Fluorescence and transmitted light traces were extracted from small cell traps, physically downstream of a larger spotting region. (B) Microscope image of cell spotting region and smaller downstream traps.



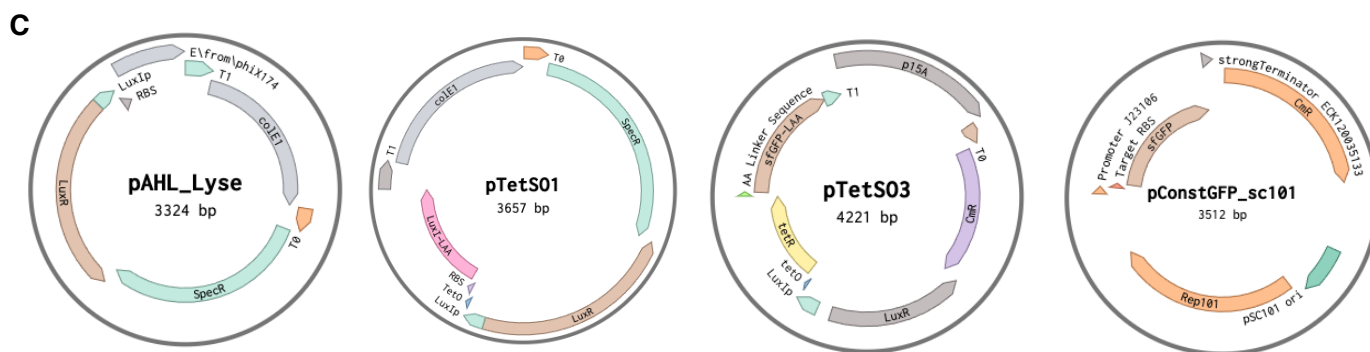
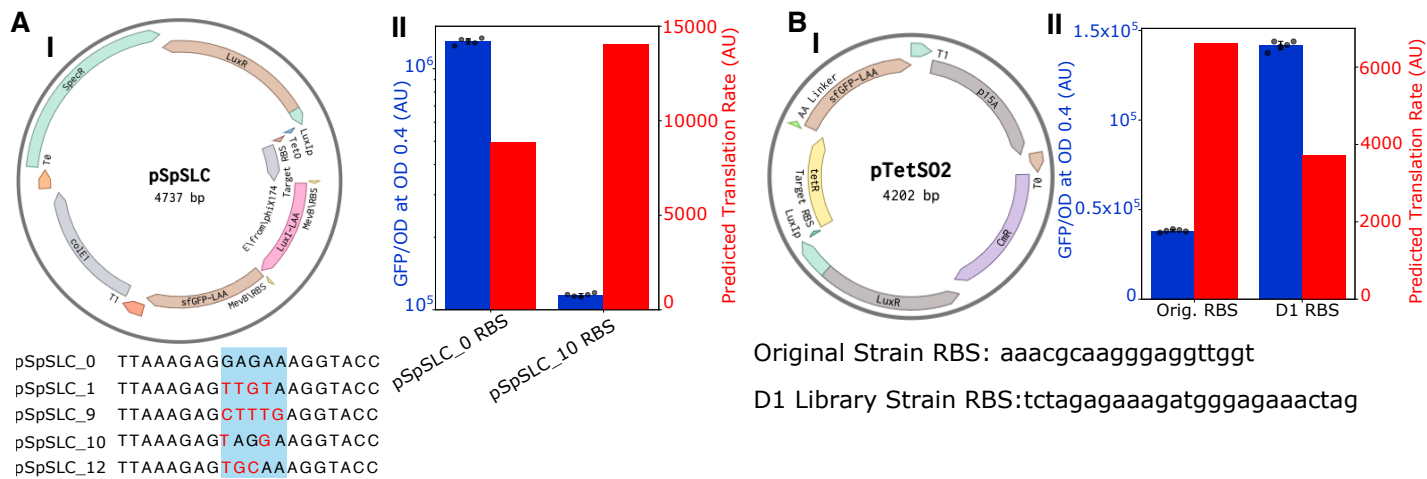
SI Figure 2: Modeling the effects of exogenous AHL and lysis Gene RBS strength on SLC oscillatory dynamics (Supplementary data related to Figures 2 and 3) (A) Modeling results showing effect of exogenous AHL on SLC dynamics. I) Cell density vs. time for different media AHL concentrations. II) Cellular AHL concentration vs. time for different exogenous AHL concentrations. III) Oscillatory period as a function of the exogenous AHL concentration. (B) Representative data used to create lysis dose response curves shown in Figure 3C and 3D. I) Lysis magnitude was calculated as the change in culture optical density (OD) during a lysis phase (L) divided by the change in OD during a growth phase (G). Light red vertical bar represents time point when 2 μ L of a 100X AHL stock was spiked into each culture well to achieve the desired AHL concentration. II) Representative growth and lysis curves used to construct the dose-response curves shown in Figure 3 for the pSpSLC₁₀ strain RBS. III) Representative growth and lysis curves used to construct the dose-response curves shown in Figure 3 for the pSpSLC₀ strain RBS. (C) Modeling the effect of lysis strength on GFP expression in the SLC. I) Normalized peak amplitude of cell density, cellular AHL, and cellular GFP for varying values of the model parameter D , the max death rate due to lysis. II) Peak GFP intensity as a function of D for varying threshold AHL values needed to trigger GFP expression, GFP_{Th} .



SI Figure 3: Analysis of P2N2-Tet Oscillator Circuit Design (Supplementary data related to Figure 4) (A) Heatmap showing representative mean GFP time traces for the original implementation of the P2N2-Tet oscillator design grown in a microfluidic device with variable trap sizes and aTc concentrations. Cell trap sizes ranged from $1.0 \times 10^{-2} mm^2$ (Large Trap) to $0.16 \times 10^{-2} mm^2$ (Small Trap). Color scale is linear and represents mean trap GFP signal (AU). (B) Modeling results for the P2N1-Tet circuit design with varying TetR expression levels (T_{Max}) for different values of the model delay parameter, τ , and the TetR repression Hill coefficient, m . I) $\tau = 1, m = 2$ II) $\tau = 1, m = 4$ III) $\tau = 2, m = 2$ IV) $\tau = 2, m = 4$. (C) Mean steady-state GFP for P2N1-Tet circuit in microfluidics for varying aTc concentrations. Error-bars represent standard deviation of 8 distinct cell traps from the four largest trap sizes pooled together. (D) Modeling results showing the impact of aTc on P2N1-Tet circuit dynamics. aTc concentrations are in arbitrary units.



SI Figure 4: Analysis of P2N2-Tet Design (Supplementary data related to Figures 4 and 5) (A) Full single strain microfluidic data set for the original implementation of the P2N1-Tet synchronized oscillator. Cell trap sizes ranged from $1.0 \times 10^{-2} \text{ mm}^2$ (Large Trap) to $0.16 \times 10^{-2} \text{ mm}^2$ (Small Trap). Color scale is linear and represents mean trap GFP signal (AU). (B) Full single strain microfluidic data set for the P2N1-Tet synchronized oscillator library strain D1. Cell trap sizes ranged from $1.0 \times 10^{-2} \text{ mm}^2$ (Large Trap) to $0.16 \times 10^{-2} \text{ mm}^2$ (Small Trap). Color scale is linear and represents mean trap GFP signal (AU). (C) The D1 P2N1-Tet strain oscillates with different frequencies based on trap size and flow rate. I, II) Representative time traces of oscillator GFP dynamics in two different cell trap sizes. Light red vertical bars indicate time point where the hydrostatic pressure driving flow was reduced from 10 to 6 inches of H_2O . III) Boxplot showing changes in period of oscillations for three different trap sizes at high and low flow rates corresponding to hydrostatic pressures of 10 and 6 inches of H_2O respectively. Box extends from first to third quartile of data and whiskers extend 1.5x the interquartile range. (D) The oscillatory properties of the P2N1-Tet strain D1 are unaffected by aTc concentrations up to 50ng/mL. I) Representative scatter plot showing mean peak-peak interval for different aTc concentrations for strain D1. Data are for the second largest trap size ($0.81 \times 10^{-2} \text{ mm}^2$) under the low flow condition referred to in panel B (6 inches of H_2O). For each concentration, error bars represent standard deviation of all measured peak-peak pairs across two replicate cell traps. II) Representative scatter plot showing mean peak-trough GFP difference for varying aTc concentrations for strain D1. Data are for the second largest trap size ($0.81 \times 10^{-2} \text{ mm}^2$) under the low flow condition referred to in panel B (6 inches of H_2O). For each concentration, error bars represent standard deviation of all measured peak-trough pairs across two replicate cell traps. (E) Modeling results showing the predicted impact of aTc on P2N1-Tet circuit dynamics. aTc concentrations are in arbitrary units.



SI Figure 5: Plasmids Used in this Study and Sequenced RBS Variants (Supplementary data related to Figures 3 and 5 (and throughout)) (A) I) Plasmid map for the synchronized lysis circuit (SLC) used in this study with lysis gene RBS sequences for selected library strains shown below. II) Comparison of experimental (blue) and RBS calculator predicted (red) expression strengths for the pSpSLC₀ and pSpSLC₁₀ RBS sequences driving constitutive GFP expression in the plasmid pConstGFP_sc101 shown in panel C. For experimental data, bar heights represents mean and error bars represent standard deviation of 5 independent cultures (individual data points are plotted with bar graph). (B) I) Plasmid map for the negative feedback plasmid used in the P2N1-Tet oscillator circuit design with TetR-GFP RBS sequences for the original strain and strain D1 shown below. II) Comparison of experimental (blue) and RBS calculator predicted (red) expression strengths for the original and D1 P2N1-Tet TetR-GFP RBS sequences driving constitutive GFP expression in the plasmid pConstGFP_sc101 shown in panel C. For experimental data, bar heights represents mean and error bars represent standard deviation of 5 independent cultures (individual data points are plotted with bar graph). (C) Plasmid maps for remaining plasmids used in this study. pAHL_Lyze was used to construct lysis dose response curves shown in Figure 3. pTetS01 was the positive feedback plasmids for the P2N2-Tet and P2N1-Tet oscillator designs. pTetS03 was the negative feedback plasmid for the P2N2-Tet design. pConstGFP_sc101 was used for the experimental characterization of RBS strength shown in panels A and B.